A Review of challenges and solution in the detection of disease in the Brinjal leaves

S. Abisha
s.abishastephen@gmail.com

S. Frank Stephen

Research Article

Keywords: Recognition, Texture, Classification Methods, Image Fusion, Discrete Shearlet Transform

Posted Date: November 27th, 2024

DOI: https://doi.org/10.21203/rs.3.rs-5415216/v1

Additional Declarations: No competing interests reported.

A Review of challenges and solution in the detection of disease in the Brinjal leaves

S. Abisha1[a,*], S. Frank Stephen2[b]
[a]Assistant Professor1, PSN Institute of Technology and Science1, Tirunelveli1, India1
[b] Assistant Professor2, St. Xavier's Catholic College of Engineering2, Nagercoil2, India2
[*] s.abishastephen@gmail.com

ABSTRACT:Crop damage and monetary losses occur due to plant diseases. At specified periods, farmers closely monitor their crops in the field to look for infections or diseases. In place of manual diagnosis, computers have been used to provide computerized tracking and recognition of a variety of diseases.This study makes a contribution to denoising algorithms that improve contrast, edge details and picture details. To isolate the leaf affected area, segmentation was carried out. Image fusion is performed using the segmented image obtained from several segmentation techniques, and features are extracted according to structural, texture, and color criteria. Furthermore, an image fusion technique based on Discrete Shearlet Transforms (DST) is applied to improve imaging quality while reducing redundancy. The color, texture, and structural elements of the fused images are retrieved and fed into the Artificial Neural Network (ANN) for classification, resulting in improved performance. When compared to other classification methods (SVM, MSVM, FFNN, and RFNN), the accuracy required for the DST-based fusion approach and the Radial Basis Function Neural Network is relatively high. The classification accuracy was 99.35%, with 89.24% sensitivity, 94.67% specificity, and 90.12% precision.

Keywords: Recognition; Texture; Classification Methods; Image Fusion; Discrete Shearlet Transform.

1.Introduction

In our nation India, 70% of people are employed in the agricultural sector. The reduction of agricultural lands and the rise in human population have forced us to consider the creation of high-yielding cultivars as well as the broad application of contemporary scientific technology. Plant diseases affect all plants from seed to maturity and since the diseases are discovered by manually when the plants' yield is severely impacted, a review of plant diseases and crop yield is necessary. Climatic variationhas an impact on the diseases, which spread in a short interval of time.Modern tools and methods may gauge their severity in relation to crop yield.Plant diseases are caused by pathogens. Though there was lack of knowledge in ancient times, the famous Greek philosopher Aristotle and plant biologistTheophrastus mentioned plant diseases in 350 BC. In the early 20th century, the American chestnut tree was affected by Asian blight disease.

Recognizing and visualizing the plant illness using the standard agricultural technique, in which the disease is verified through isolation process. While pathogens identification and treatment are becoming more and more common in engineering sectors, they are relatively new in agriculture. The rate at which foliar diseases are detected by image processing is gradually enhancing. In wide areas, disease identification with the naked eye is both insufficient and inefficient. Image processing is a useful tool that farmers can employ to monitor crop development and diseases detection technique is more effectively than simple eye observation. The primary focus of the work is to identify plants disease using recognition and classification.

- The denoising algorithm improves contrast, edge details, and picture details. By using a proper technique, the leaf's affected area can be isolated by using segmentation. Image fusion is carried out by using the segmented image by various segmentation techniques.
- According to the study, a variety of features including structural, texture, and color can be extracted.
- Different forms of classification are suggested in the plant disease detection using leaf recognition stage. Three well-known classifiers, notably SVM, MSVM, FFNN, and RFNN, are employed.

The rest of the paper is arranged as follows:The work that has already been done was covered in Section 2, and image preprocessing and segmentation techniques were presented in Section 3. Image Fusion is covered in Section 4. The development and complexity of brinjal plant diseases are examined in Section 5 using color, texture, and structural feature descriptors. In Section 6, the diseases in brinjal leaves are categorized using image classification techniques as SVM, MSVM, FFNN, and RFNN. The results are discussed and examined in Section 7.

2.Literature Review

Tuker and Chakraborty (1977) hypothesized diseases in sunflower and oat leaves based on detection techniques. The suggested algorithm and the affected area in this strategy have better outcome. Sometimes mistakes happen when taking pictures because of bad lighting. Although Ostu's segmentation approach and K-means clustering are used, the resulting images have a very low Mean Square Error. Anand et al. (2016) segmented the brinjal leaves using K-means clustering. After determining the threshold value, Skaloudova et al. (2016) suggested a method to distinguish the leaf from the background image and separate the affected area from the healthy portion. The double threshold approach was compared to the other existing methodologies, which included the leaf damage index and chlorophyll fluorescence. It was discovered that, in comparison to other approaches, the double threshold method produced superior results. Youwen et al. (2008) created support vector machines using image processing to identify and distinguish between different types of cucumber leaf diseases. The noise was initially eliminated using a vector median filter. Segments of the affected leaf images were obtained using mathematical morphology and statistical pattern recognition. In the end, the diseases were categorized using SVMwhich yielded superior resultsafter the shape, texture, and color were retrieved.

Muthukannan et al. (2015) used a method based on fuzzy edge and clustering segmentation for a variety of plant-related investigations. Prior to segmentation, preprocessing techniques such as picture modification, morphological operations, diminishment via middle channel, and disturbance were carried out. A linear polynomial approach was presented by Ajiet al. (2013) as a way to reduce the processing time for foliar diseases of palm oil leaves. This method achieved an accuracy of 87.75% in the classification process by employing neural networks to extract features from affected leaves for disease categorization. Barbedo et al. (2014) established the threshold method and color analysis to identify the disease on leaves. The proposed algorithm shows symptoms and limitations of pixel miscalculation error and system robustness with variation in size, shape and color.Reverse Propagation by Orillo et al. (2014) suggested the Artificial Neural Network (BPNN) to identify rice leaves associated with various diseases. This approach carries out feature extraction, image segmentation and image enhancement. Pomegranate leaf disease was detected by Bhange et al. (2015) using an online tool. Following feature extraction, SVM and K means algorithms were applied to separate the affected area from the healthy portion. This approach yielded an accuracy achievement of 82%. Singh and Misra (2017) advocated the application of genetic algorithms for automatic detection and classification of plant diseasesfrom healthy leaf portions. According to recent studies,Machine vision has a bigger role in agriculture, which should be further investigated. No significant efforts have previously been made to detect the severity of the disease at different stages, which has an impact on the nation's and the farmers' economies.

3.Methodology

The proposed methodology for the disease detection and recognition of the collected brinjal plant using the image processing technique is shown in Figure 1.

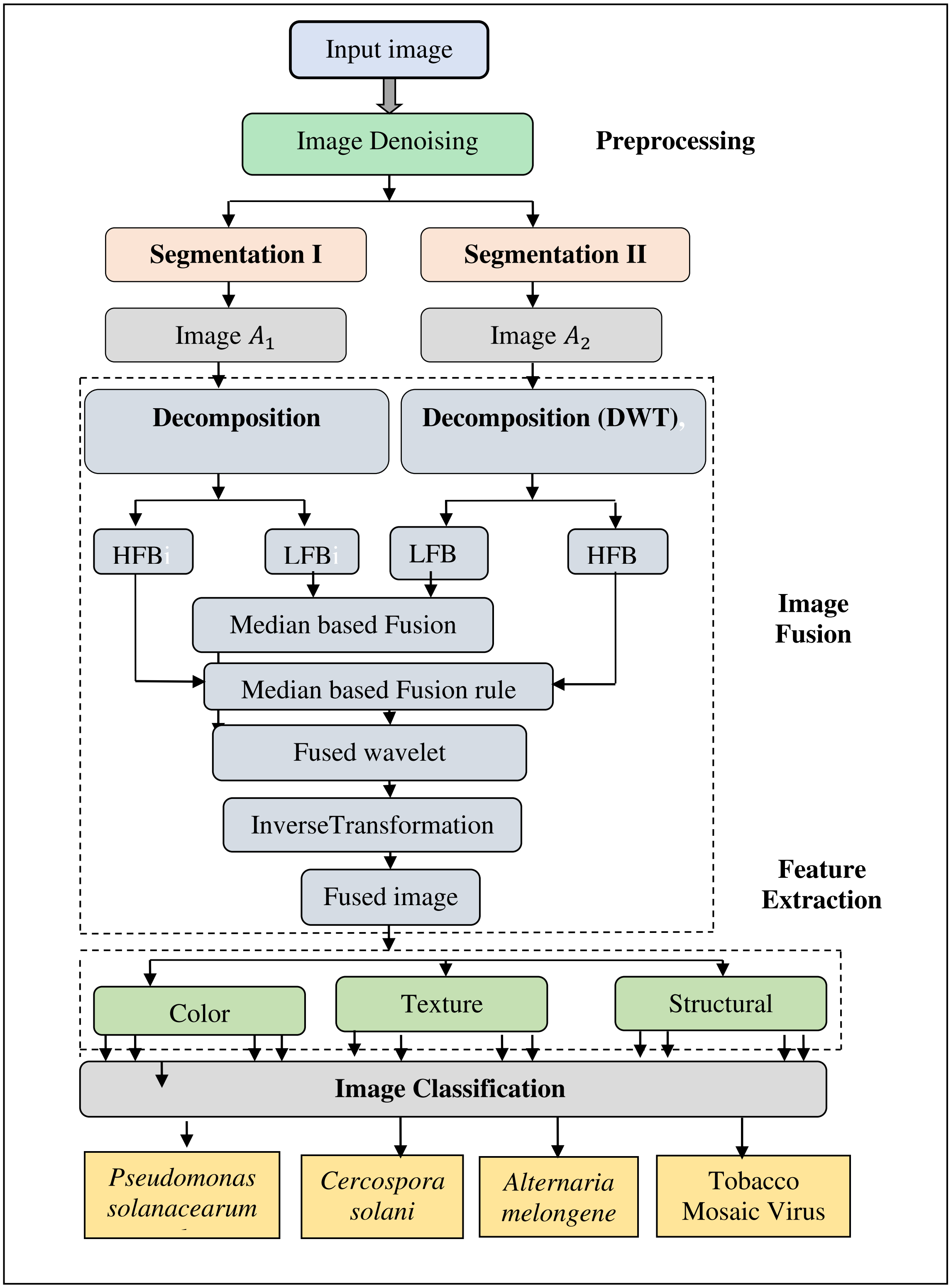

Fig. 1. Block diagram for diseases detection in brinjal leaves.

3.1. Image Processing

In image processing, specific information can be recovered by removing noise from the raw leaf images by fix geometric distortions and provide a more accurate depiction.The collected image for the disease detection is shown in Figure.

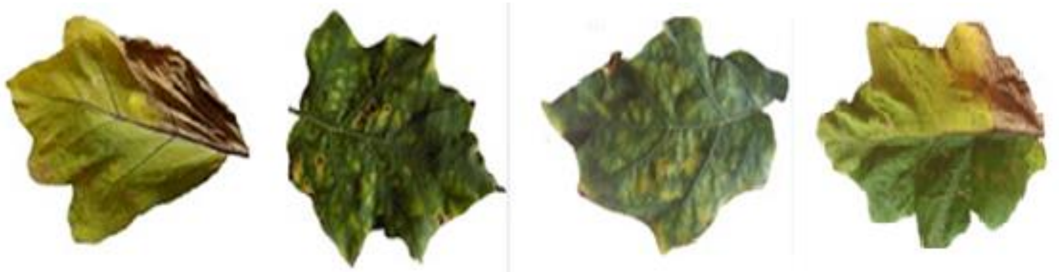

Fig. 2. Different set of brinjal infected leaf.

Image denoising and image segmentation are the two main crucial phases in preprocessing. To acquire correct image details, the first step in denoising is to suppress noise and remove extraneous information. There is additive or speckle noises present in the leaf. By eliminating high frequency components and adjusting the original leaf image to obtain low frequency, image denoising smoothed leaf image. The brinjal leaf contaminated area is subjectedto segmentation stage, which involves removal of the leaf image from its background (i.e., the region of interest).

3.1.2. Fuzzy C means segmentation

Fuzzy clustering algorithm introduced by James et al 1984 is one of the most important techniques. While diminishing a membership function, a range of data points is partitioned using the FCM algorithm. Assume that, $X = \{x_1, x_2 \dots x_m\}$ represents the set of diseased leaves and n is the total number of sample points. Letμ_{mn}be the degree of membership in the n class that satisfies the condition mentioned below:

$$\sum_{a=1}^{m} \mu_{ab} = 1 \tag{1}$$

The fuzzy C Means is focused on iterative minimization of the below-mentioned objective function.

$$O(M, C) = \sum_{a=1}^{c} \sum_{b=1}^{m} \mu_{ab}^{l} |x_b - C_a|^2 \tag{2}$$

$x_1, x_2 \dots x_m$ is a vector for infected samples. Let C={ $C_1, C_2 \dots C_a$} be the cluster center and $U = \{\mu_{ab}\}$ be $M * N$ matrix where$\mu_{mn}$is the mth membership value of the nth leaf collected in the samplex_b. The following constraints are applied to membership function.

$$0 \le \mu_{ab} \le 1 \quad a = 1,2, \dots c; \quad n = 1,2, \dots . m \tag{3}$$

For estimating the cluster center, all leaf samples are taken into account, as well as the samples was weighted using membership functions. Each leaf sample's, membership value for each class is determined by its distance from the relevant cluster center. The steps of the FCM algorithm are as follows.

(1) The number of clusters arechosen from the fuzzifier $0 \leq l \leq \propto$, Set up the membership matrix $\cup^0$ such that $\mu_{ab}^0 = 1, a = 1,2, \ldots c;\ \ b = 1,2, \ldots . k$are not equal.

(2) Cluster center is to be calculated.

$$C_m = \frac{\sum_{b=1}^{m} n(\mu_{ab})^l}{\sum_{b=1}^{m}(\mu_{ab})^l} \tag{4}$$

(3) New membership function based on cluster centercan be calculated

$$\mu_{ab} = \frac{1}{\sum_{p=1}^{c}\left(\frac{\|x_b - c_a\|}{\|x_b - c_p\|}\right)^{2/_{l-1}}}; \qquad a = 1,2, \ldots c;\ \ b = 1,2, \ldots . m \tag{5}$$

(4) Compare $\cup^{n+1}$and $\cup^n$, if $|\cup^{n+1} - \cup^n| < \in$go to step 2, otherwise to step 2; where $\in$ is lowest permissible change in $\cup$.

In the membership function of the FCM method, each leaf sample x_n appears only once and the membership function is clearly decreased if each sample is linked with its closest cluster centre. As a result, x_b is assigned to the class ‘a’. Ensuring that $\|x_b - c_a\|$ is the smallest when a=p. The cluster center is determined based on the minimize n after the leaf samples have been regrouped. The operation can be repeated until the predetermined value can no longer be registered.

3.1.3. K Means clustering algorithm

Using large datasets, unsupervised clustering technique moves the partition from one cluster to the next, beginning with the initial partitioning (Singh et al 2017). 'n' observations are divided into 'k' clusters by explicitly stating and initializing the cluster numbers. The cluster centers are chosen at random, and the datapoints are used to compute the distance between the cluster center and the image datasets. By converting each datapoint into a cluster with the smallest distance between them, the centroid value was recalculated. Each centroid is matched to a single data point, and the process is repeated until the centroid does not move further, resulting in a gradual change in the centroid value.

Steps of a K Means clustering algorithm are as follows.

Step 1: Initialize the K centroid vectors arbitrarily.

Step 2: The dataset is given to the closest centroid vector in every point based on the Euclidean distance among each datapoint and every cluster center formula is calculated using equation (6).

$$K(d_o, c_r)\sqrt{\sum_{k=1}^{n}(d_{oe} - c_{re})^2} \tag{6}$$

Where $d_o$signifies oth data vector and c_r indicates the centroid vector of cluster r and e subscripts for every centroid vector.

Step 3: Using the equation (7), the cluster centroid vectors are re-estimated.

$$kD_r = \frac{1}{n_r}\sum C_{vr} \in d_o \tag{7}$$

where C_{vr} represents the centroid vector, n_r is the number of data vectors in a cluster and d_o is the subset of data vectors until a stopping criterion is satisfied. Convergence based on objective function minimization and Mean Squared Error could be calculated as follows:

$$MSE = \sum_{I=1}^{A} \left\| S_j - C_r \right\|^2 \quad (8)$$

where $S = \{s_1, s_2, \dots \dots s_a\}$; Cluster centroids is $C = \{c_1, c_2, \dots \dots c_a\}$.K Means clustering method operates on the initial centroid vectors, which are generated randomly. Without adequate initialization, the formation of the final center causes major problems, and there is a course of many dimensions in every feasible value in order to boost accuracy and efficiency.

3.1.4. Expectation Maximization Segmentation

EM segmentation is an aggressive method based on a model based approach. A parametric distribution can be used to represent each region in a Gaussian model. A Gaussian mixture model is a density model with a large number of component distributions. To represent an object's colors in order to accomplish tasks such as real-time color segmentation.In the following equation, parameters like mean and covariance matrix are used to determine the Gaussian density for a set of all data points for a 1D vector measurement $X = \{x_1, x_2, \dots., x_j, \dots., x_b\}$. In a Gaussian mixture model, equation (9) gives the most likely distribution-based density for the leaf image.

$$p(x_j/\theta) = \sum_{k=1}^{e} a_e(x_j | \varphi_e) \quad (9)$$

Component should satisfy $a_e > 0$, where a_e is the weight of the mixture based on the prior probability. The value of MAP in E step with respect to the infected part of the image is based on joint density function, which can be initialized using the Bayes rule algorithm.It computes the conditional expectation of the data point within the region to determine a posterior probability.

$$p_{ej}^{(d)} = \frac{a_e^{(d)} G(x_j | \varphi_e^{(d)})}{\sum_{e=1}^{k} a_e^{(d)} G\left(x_j \middle| \varphi_e^{(d)}\right)} \quad (10)$$

The M step has been used to maximize the expected value, and the means are determined as follows:

$$\mu_e^{(d+1)} = \frac{1}{\sum_{j=1}^{n} p_{ej}^{(d)}} \sum_{j}^{n} p_{ej}^{(d)} x_j \quad (11)$$

Even though, segmented image performs better in this segmentation, but orientation near the boundary and edge significant disadvantages. To overcome this restriction Automatic Spectral based lesion segmentation is performed.

3.1.5. Automatic Spectral based lesion segmentation

The automatic spectral based lesion segmentation procedure consists of three steps: gridding, choosing a pixel mask, and applying ROI. Gridding is a technique that creates smaller size of images in a single leaf image by drawing an imagined grid over it. The four sections of the square-shaped grids are four, eighteen and twenty-four. Each grid is divided by using the masking technique. The histogram is analyzed for each pixel inside the grid and the pixel mask is determined by selecting the value with the highest peak. The lesion area is then expanded. To determine whether the surrounding pixels satisfied the restrictions, the pixel mask was compared to next grid.The restrictions have to meet the standards for orientation and intensity threshold. The intensity threshold displayed the greatest amount by which the value of the subsequent pixel has deviate from the previous pixel's value. Assume that the intensity threshold is set to T, that the neighboring pixel and pixel mask have an intensity value. Additionally, assume that the intensity constraint has been satisfied whenever the difference in intensity between the neighboring pixel and the pixel mask falls within the threshold's range. Then compute the gradients on both the x and y axes to determine the orientation restriction.

Let $G_a$be the gradient value when applying the gradient in the x axis, and G_b be the gradient value once applying gradient in the y axis. The gradient value is expressed in radians, which are then translated to degrees, with orientation values ranging from 0 to 180. Using the formula in the following equation (12), both values are grouped to generate a gradient matrix G.

$$G = \frac{1}{1 + ({G_a}^2 + {G_b}^2)} \tag{12}$$

When a mask and its surrounding pixel meet the requirements for both orientation and intensity, the lesion area is increased by adding the nearby pixel to the region. ROI carries out the precise lesion region detection. The images taken in the field can be categorized into non-extensive and extensive scenario based on the distinct border criteria between the lesion place and the surrounding areas. In the non-extensive, the lesion point is connected to image boundaries on one or both sides of the leaf, but in the extensive scenario, the lesion area is positioned in the center of a leaf image without being tied to any borders. The equation (11)is used to separate the lesion boundaries from the leaf image energy difference parameter.

$$D_{ab} = \frac{|A|A \in I(a,b), A \in B_s|}{\sqrt{|A|A \in I(a,b)|}} \tag{13}$$

A is the location in the leaf image, and $B_s$is the collection of boundaries within the leaf image. The color difference between two colors a and b can be calculating from the R, G and B component values.

$$\Delta E = \sqrt{(R'_1 - R'_r) + (G - G'_r) + (b'_1 - b'_r)} \tag{14}$$

where, $\Delta R' = R'_1 - R'_r$, $\Delta G' = {G_1}' - G'_r$, $\Delta b' = b'_1 - b'_r$

The RGB color space is defined by three channels of the input image $\Delta R'$, $\Delta G'$ and $\Delta B'$and R'_r, G'_r and B'_r are denoted as the RGB color space and $\Delta R'$represents the difference among green and red. The difference among green and blue is represented by $\Delta G'$. and the difference among red and blue is represented by$\Delta B'$.

2. The binary image I_{bi} is produced in the equation (15) by apply the threshold T to the input image I_{im}.

$$I_{bi} = \begin{cases} 1, & if I_{im} \leq T \\ 0, & otherwise \end{cases} \tag{15}$$

3. The subsequent elements of the segmented image are multiplied with the original image to obtain the coloured segmented image as in equation (16)

$$I_{rgb_{seg}} = I_{bi} \circledast I_{im} \tag{16}$$

where $\circledast$ is the multiplicative operator, $I_{bi}$is the segmented binary image. The input image is$I_{im}$and the output image is$I_{rgb_{seg}}$is the output image. This technique solves all the problem in the existing methods and is ideally suited for large dataset images with small lesion regions and boundaries.

3.2. Image Fusion

3.2.1. Discrete Wavelet Transform based fusion

Discrete Wavelet Transform based fusionis provided to combine all important information from segmented image into a single image. This method finds the best suited for machine intelligence perception while also reducing the amount of data. The key phases in DWT-based fusion are as follows:

Step 1: First, we segmented the two images using Automatic Spectral Lesion and EM segmentation as $B_1$and B_2. These images are subjected using discrete wavelet transform to produce the complex coefficient sets D_1 andD_2.

Step 2: The median values for each coefficient are specified by decomposition level forming 3*3 window.

Step 2:To evaluate the absolute difference between each coefficient is determine by matching the median value by using the equation (17) and (18).

$$E_1 = |median_1| - |D_1| \tag{17}$$

$$E_2 = |median_2| - |D_2| \tag{18}$$

Step 4: A coefficient set for the fused image is created by comparing the absolute differences of the coefficients from the two segmented images and the largest absolute difference coefficient is selected from the median.

$$\mathrm{D}(i,j) = \begin{cases} D_1\, if\ |E_1| \geq |E_2| \\ D_2\, if\ otherwise \end{cases} \tag{19}$$

Step 5: Finally, the fused infected images are created by applying an inverse discrete wavelet transform on fused coefficients set.

3.2.2.Dual Tree Complex Wavelet Transform (DTCWT)

A directional wavelet transform with a shift variation is the Dual Tree Complex Wavelet Transform (DTCWT). The DTCWT and its inverse DTCWT are implemented using analysis and synthesis filter banks. The input leaf images are converted into a set of low frequency coefficients (L) or high frequency coefficients (H) is given in the equation (20).

$$(L, H) = DTCWT(B) \tag{20}$$

The approximation coefficientsM_1 *and* $M_2$are fused using the median fusion rule and detailed coefficients $I_1, I_2$are joined using the median fusion rule to form a single set of coefficients equivalent to fused pictures and determined by the following equation.

$$M_f = \alpha_l(L_1, L_2) \tag{21}$$
$$e_f = \alpha_d(I_1, I_2) \tag{22}$$

Where the fusion rules for low and high frequency coefficients are denoted by I_1 and I_2 respectively. Figure 3 shows the merged high and low frequency coefficients, $M_f$and E_f. Equation 23 is used to utilize inverse DTCWT on M_f and E_f to transform the fused coefficients into a fusion image (A).

$$A = IDTCWT(M_f, E_f) \tag{23}$$

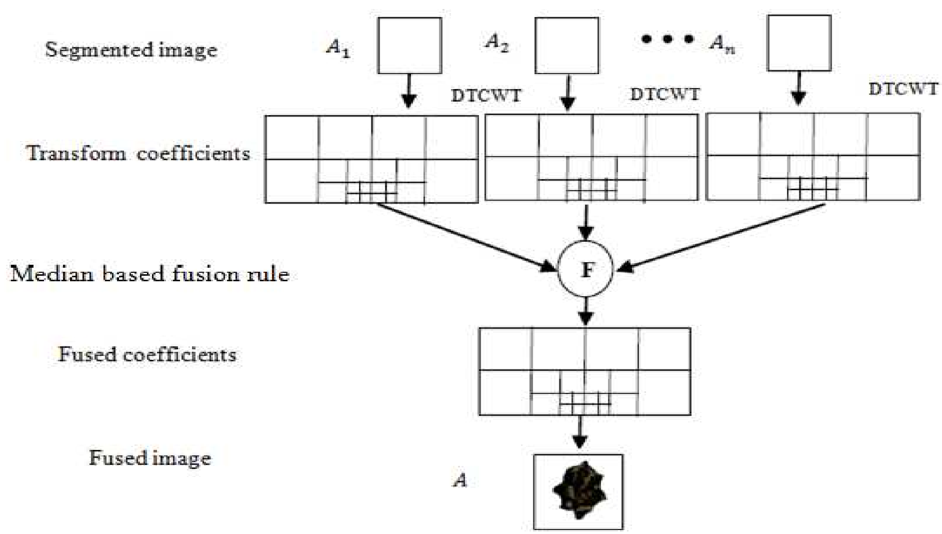

Fig. 3. Dual tree complex wavelet transforms

3.2.2. Discrete Shearlet Transform

The most sophisticated method for showing multidimensional data seems to be the shearlets. The shearlet follows the parabolic scaling law and is very efficient even in the marginal boundary areas. Each parabolic scale doubles the range of directions. Shearlet parameters serve as the function for the scaling parameter "a," shearlet parameters, and translation parameter "tr.". This parameter is used to find the best spare approximation.$\varphi_a: a > 0, S \in \gamma, tr \in \gamma^2$. The matrix $M_a$can be expressed as

$$M_a = S_a P_a \tag{24}$$

where Shear matrix represent as S_a and parabolic scaling matrix is represented asP_a

$$S_a = \begin{pmatrix} 1 & s \\ 0 & 1 \end{pmatrix} \tag{25}$$

$$P_a = \begin{pmatrix} a & 0 \\ 0 & \sqrt{a} \end{pmatrix} \tag{26}$$

Then Shearlet Transform is defined as,

$$ST = \langle f, \varphi_a \rangle \tag{27}$$

The pyramid transform is used to accomplish the multiscale subdivision of the shearlet transform. By replacing the convolution process, the shearlet transform introduces shift variance and makes advantage of the Gibbs phenomenon, which produces edge smoothness. The following step uses shift invariant filtersis used to achieve directional localization. There are several trapezoidal high frequency sub bands and low frequency sub bands that make up the frequency plane. The pyramid transform would be used to further partition the low frequency subband. Until the necessary degree of decomposition is achieved, the process is repeated. Figure 4.depicts the Discrete Shearlet Transform's basic structure.

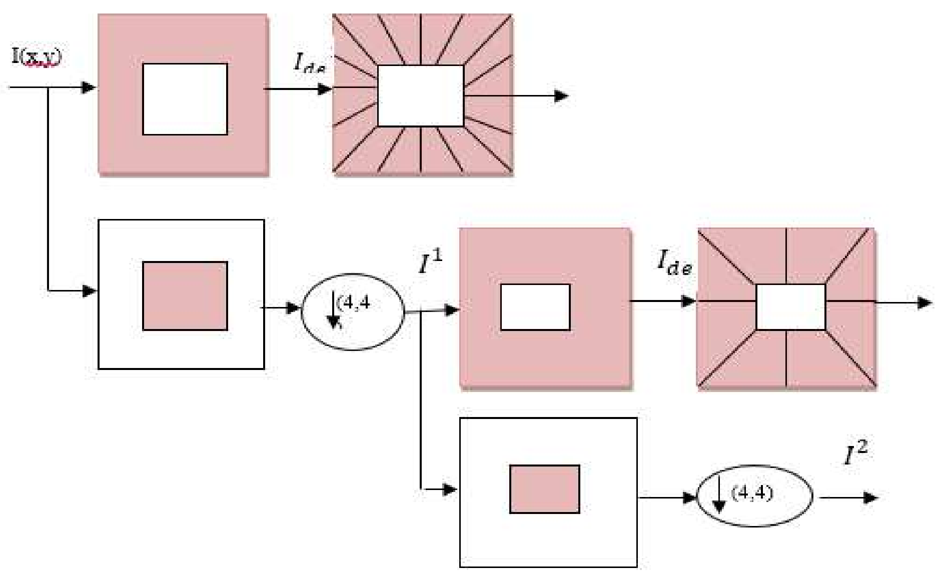

Fig. 4. Structure of Discrete Shearlet Transform.

There are two steps are involved in the image decomposition process using a Discrete Shearlet based transform. The shear matrix X_0 or X_1 is used to decompose the image in several directions and to produce the multiscale decomposition of each direction of the image.If the image is decomposed either by X_0 or $X_1$the number of directions is expressed as $2(l + 1) + 1$. If the image is decomposed both as X_0 and X_1, then the number of direction given in $2(l + 2) + 2$.

3.3. Feature Extraction

In order to characterize the visual feature extraction process, high level information is obtained. The main elements present in the image are color, shape and texture. Texture is an important characteristic in disease diagnosis since it helps to identify the area of the leaf that is affected. The matrix NX_d specifies the relationship among segmented and neighbour pixels at a given moment NX_d. Co-occurrence matrix is used to identify the texture feature in two steps.

1. The $E(i,j)$ matrix of I (the initial pixel) and j (the matching pixel) located at a distance D is used to count the pair of pixels.
2. At the i^{th} row and j^{th} column of the matrix, the estimated count is entered.

One of the most effective and dependable methods that image pathologists employ to identify and categorize lesion areas is the ABCD structural rule. The four main parameters are Asymmetry, Border Color, and Diameter. Because of the asymmetry of the lesion, several forms of diseases in brinjal can be identified. The lesion area is divided along the major and minor axes to find the asymmetry value.

$$\text{Asymmetry index} = \frac{\mathrm{N}_1 + \mathrm{N}_2}{\mathrm{N}} \qquad (28)$$

Where $N_1$and N_2 are the overlapped regions along the minor and major axis of the lesion respectively and N is the total area of the lesion spot.

Different colors including red, white, light brown, dark brown, green and yellow are present in the lesion spots. A score of '1' is assigned to each hue for execution. The maximum score range is '1' and the lowest score is obviously '0' when every color is represented in the lesion region. The image is converted from RGB model to CIE Lab color space in order to verify whether one or more colors are present in the leaf lesion area. This is due to the fact that, in contrast to the CIE lab models, the RGB color models distance between these two hues does not accurately represent the actual difference that the human eye would perceive. The difference in between estimated valueis measured using the Euclidean distancein the equation 29.

$$D = \sqrt{(\mathrm{R}_2 - \mathrm{R}_1)^2 + (\mathrm{G}_2 - \mathrm{G}_1)^2 + (\mathrm{B}_2 - \mathrm{B}_1)^2} \qquad (29)$$

where, R_1, G_1 and B_1indicate the desired color's components in the CIE Lab colour space, andR_2, $G_2$and B_2represent each pixel in the lesion image.

3.4. Image Classification

3.4.1. SVM and MSVM

One effective supervised learning technique is SVM. It uses tagged training data to create an input-output mapping function. SVM is a widely used pattern recognition technique. The main concepts of SVM are to create a feature vector and then use that feature vector to transfer kernel functions into a feature model. Lastly, training vectors are classified using the feature space. The main advantage of SVM in higher-dimensional feature space is that a kernel function can determine the hyperplane separation in place of a transformation to find the separating hyperplane. Moreover, the solution found in support vectors is the weighted sum based on the kernel functions. By increasing the accuracy rate, the kernel functions and important parameters can be selected. SVM classifiers are constructed using kernel functions in two stages:

Step :1 Using kernel-appropriate functions, partition of input features space into a higher dimensional features space. The SVM creates the maximum hyperplane margin in that feature space using a radial basis function due to the limited and localized responses throughout the entire region. In terms of precision, kernel functions are defined as,

$$k(a,b) = \exp\left\{\frac{-\|a-b\|^2}{2\rho^2}\right\} \tag{30}$$

Step :2 The SVM uses the radial basis function in that feature space to create the maximal hyperplane margin because of the finite and localized responses across the complete region. A more sophisticated version of SVM is MSVM. There are two types available: one is that, to stops all forms of breakdown and another to stop all the particular kind. SVM models are used to construct one-against-all strategy for an N-class diagnostic that separates the sample leaf from every other class. Using all of the learning techniques, the kth SVM classifier is trained, with the k^{th} class augmenting positive labels in certain scenarios and negative labels in others. To categories the leaf pictures, the Gaussian RBF kernel generates 'N' hyperplane at the conclusion. As indicated in Figure 5, a single class of approach is separated from other categories of approach hierarchically.

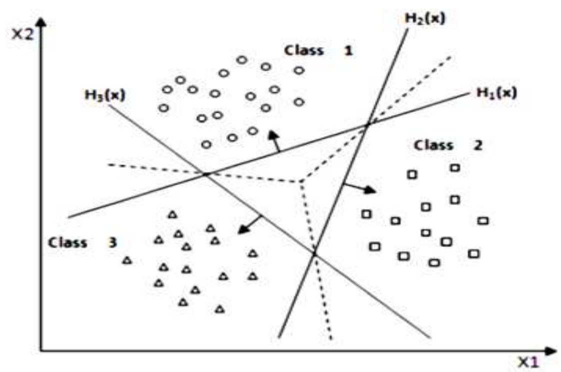

Fig. 5. Multiclass Support Vector Machine

Based on the decision value for each data object, the MSVM is trained using all of the training sets that have positive labels and all of those that have negative labels. By creating a mapping function from the input space and optimizing the kernel function parameters, nonlinear decision hyperplane surfaces are built in the input space. In the OAA method, all other classes are assigned to fast cross validation, but only one class is assigned on it. Furthermore, one student is assigned to the second class, and all other students are assigned to the other classes, and so on. Lastly, the leaf pictures are separated using the MSVM. An MSVM classifier is utilized to construct the kernel parameter selection by utilizing the OAA decomposition approach. For generalization, 10-fold cross validation estimates are used to modify the hyperparameters. A dataset of 500 leaf images is included. Two-thirds of the leaf extract from each class is given to the training set, and one-third of the leaf samples from each class is given to the testing set. The pattern x_i is denoted in N dimensional space and its label attains a value from a set according to

$$Z_i = arg \max_j h(A_i)\alpha_i + \alpha_{0i} \tag{31}$$

3.4.2.Feed Forward Neural Network

A dataset is an assortment collected images based on diseases in five output classes: low and high intensity tasks as well as healthy leaves with unknown disorders. Thirteen texture features, three color features, and four structural features were extracted from the merged images to aid in the diagnosis of different diseases. To represent five diseases, the FFNN classifier makes use of epoch 4500, 20 input neurons, an intermediate hidden layer and 5 neurons in the output layer. The back propagation algorithm was picked up in the network. Figure 6, depicts the structure of Feed Forward Neural Network.

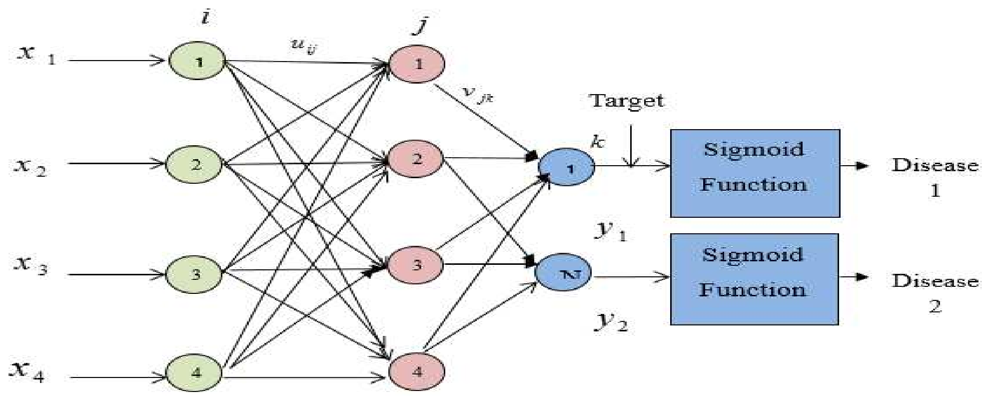

Fig. 6. Structure of Feed Forward Neural Network.

The FFNN network has better classifier performance when compared to all other machine learning techniques. FFNN offers better precision, specificity, and sensitivity than SVM.

3.4.3. Radial Basis Function Neural Network

As seen in Figure 7, the radial basis function (RBF) in a neural network consists of two layers: an output linear n^2 layer and a hidden layer of n^1 layer. A vector with n^1 entries is the outcome of the distance measure whenever it receives the input vector p and the input set of weights w_1.All of these components are vector distances, denoted as$1 \times w_1$, which are constructed from the rows of the input weight matrix. The output is merged using the multiplication operation, and element-by-element multiplication is carried out using the bias of b_1. Through the output a_2.

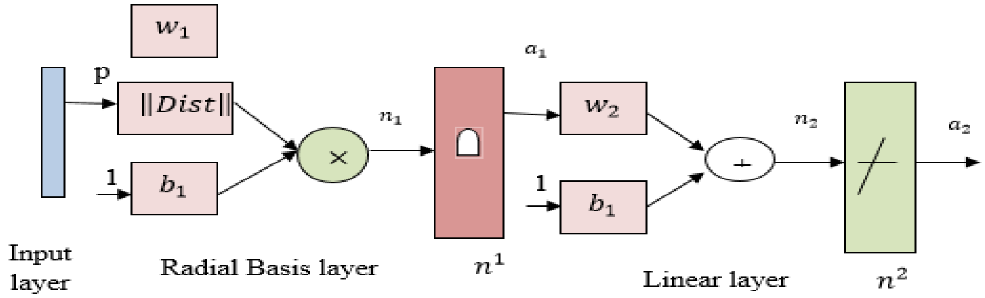

Fig. 7. Structure of Radial Basis Function Neural Network.

The output value of each neuron in the radial basis neural layers is close to the input vector. The radial basis neural network's weight vector-based output is nearly zero, in contrast to the input vector. A little output is produced by the linear output neural utilizing the linear transform function, while a value close to 1 is produced by the radial basis neuron whose weight vector is near the input value p. During the startup process, it is utilized to modify the weight and biases.

Step 1: Random weights are set up for the first time.
Step 2: Initialize the momentum factor as well as learning rate parameter with random values.
Step 3: If the requirement is not satisfied, repeat steps 32-46.
Step 4: Repeat steps 5–10 for the samples training dataset vector pair.
Step 5: These input features $i_a$which is provided as the hidden layer are received by each input layer.
Step 6: The hidden layer units $z_b, b = 1,2, \dots p$ are used to sum up the weighted input features.

$$z_{-inb} = v_{ob} + \sum_{a=1}^{n} i_a v_{ab} \tag{32}$$

The Gaussian activation method is designed to the net input features derived using the equation

$$z_b = f(z_{inb}) \text{ i. e, } f(z_{inb}) = e^{z_{-inb}^{2}} \tag{33}$$

and these features are sent to every units in the layer beneath, i.e. output units.S

Step 7: Calculate the net input for each output unit $(j_v, v = 1,2 \dots m)$using:

$$j_{-inc} = w_{ov} + \sum_{y=1}^{p} z_a w_{bv} \tag{34}$$

and calculate the output value using Gaussian activation function on the net input layer:

$$j_c = f(j_{inc}) \text{ i. e, } f(j_{inc}) = e^{j_{-inc}^{2}} \tag{35}$$

Step 8: Each output unit $(j_c, c = 1,2 \dots m)$then receives the target sample equivalent to an input sample inaccuracy (between output and concealed) that is determined using the equation,

$$\delta_c = (t_c - j_c) f'_{-inc} \tag{36}$$

Step 9: Every hidden unit $(z_y, y = 1,2 \dots n)$ adds the delta input feature values from units inside the layer above to get delta input feature value:

$$\delta_{-inb} = \sum_{c=1}^{m} \delta_b w_{bc} \tag{37}$$

The error between the hidden and input layers is calculated as follows:

$$\delta_b = \delta_{-inb} f'_{-inb} \tag{38}$$

Step 10: Determine the adjusted weight in between output unit and the concealed unit, as follows:

$$_{bc} = \alpha\delta_c z_b + \mu\Delta w_{bc}(old) \quad (39)$$

This bias term is then updated and provided by,

$$\Delta w_{oc} = \alpha\delta_c + \mu\Delta w_{oc}(old) \quad (40)$$

Step 11: Calculate the revised weight between both the hidden and input units as follows:

$$\Delta v_{ab} = \alpha\delta_b i_a + \mu\Delta v_{ab}(old) \quad (41)$$

In addition, the bias term has been revised and is provided by,

$$\Delta v_{ob} = \alpha\delta_j + \mu\Delta v_{ob}(old) \quad (42)$$

Step 12: Every output unit $(j_v, v = 1,2 \ldots m)$ adjusts its bias & weights $y = 1,2 \ldots p)$ and are given by,

$$w_{bc}(new) = w_{bc}(old) + \Delta w_{bc} \quad (43)$$

$$w_{oc}(new) = w_{oc}(old) + \Delta w_{oc} \quad (44)$$

Step 13: Each hidden unit $(z_b, b = 1,2 \ldots n)$updates its bias as well as weights $a = 1,2 \ldots n$ which are determined by,

$$v_{ab}(new) = v_{ab} + \Delta v_{ab} \quad (45)$$

$$v_{ob}(new) = v_{ob}(old) + \Delta v_{ob} \quad (46)$$

Step 14: When the algorithmic process reaches an iteration with the lowest MSE value, it should be stopped.

4. Result and Discussion

Brinjal leaflet images from different locations were gathered and used as datasets for this study. The leaves were collected is based on ill and healthy from Kerala State (Neyathinkara) in India as well as from Nagercoil, Valliyoor and Panakudi in southern Tamil Nadu and Hosur in northern Tamil Nadu. Healthy brinjal leaves (500), *Pseudomonas solanacearum* (250), *Cercospora solani* (220), *Alterneria melongenea* (230), and Tobacco Mosaic Virus (200). In Figure 8, the sample leaves are shown.

Fig. 8. Different Set of infected Brinjal leaves

In order to decrease processing speed and computing time, the image is shrunk to 256*256 resolution. A range of filters are applied to further denoise the scaled image. The noisefree photo quality was evaluated using Mean Square Error and Peak Signal to Noise Ratio, as depicted in Figures 9 and 10.

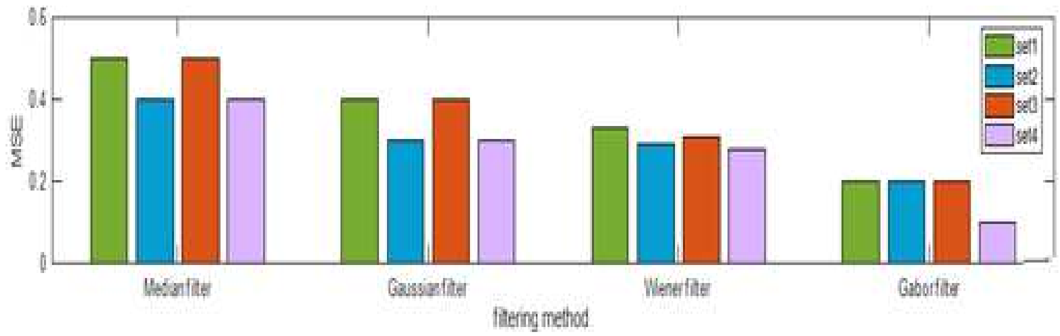

Fig. 9. Mean Square Error

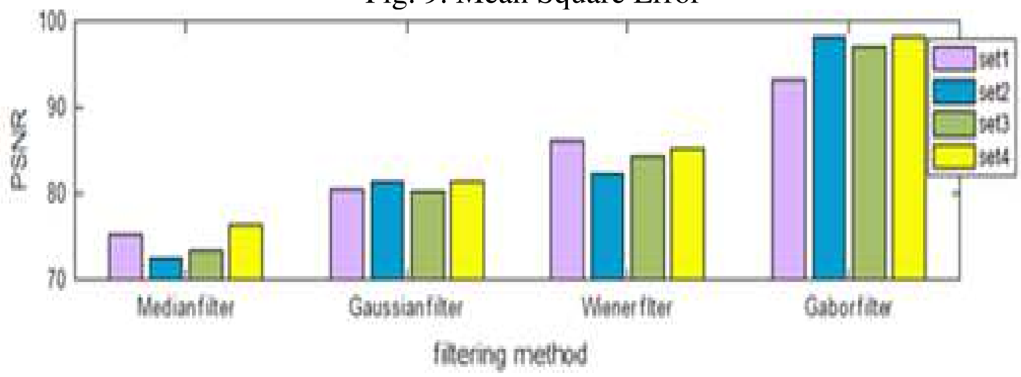

Fig. 10. Peak Signal to Noise Ratio

Compared to the Wiener filter, the Gabor filter seems to have a greater effect on the MSE. In addition, the Gabor filter has improved the smoothing and eliminating the blurring effect of the image when compared to the Gaussian, Median and Weiner filters. By assessing the PSNR and MSE for each of the four filter methods is applied for five categories of diseases. The PSNR of the Gabor filter is greater than the PSNR of the Weiner, Gaussian and median filters. A high PSNR value is obtained using the Gabor filter when the MSE is small. It offers an image of better quality. FCM segmentation is performed for many kinds of diseases, as Figure 11 illustrates.

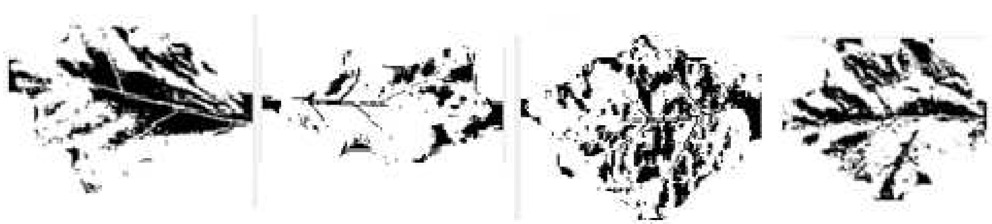

Fig. 11. FCM based segmentation

Only bimodal intensity distributions are appropriate for this model (FCM), although it is easy and quick to apply. But this method is not visible for identification of disease in brinjal leaves. Next segmentation results are displayed in figure 12, after the brinjal leaves are clusters using the K means approach.

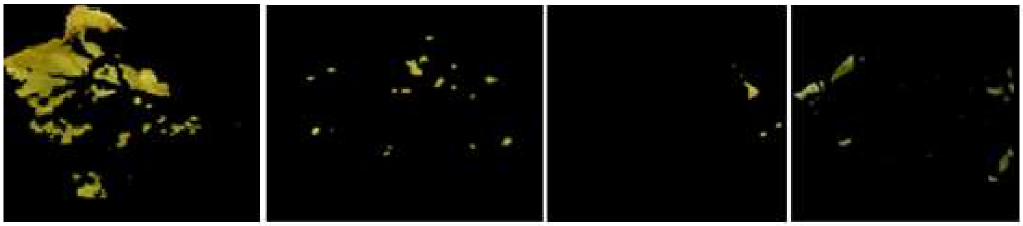

Fig. 12. K means Clustering based segmentation.

The next segmentation method eliminates the noisy spot and avoids some noise sensitivity by using FCM segmentation; nevertheless, it has a drawback in that the cluster model,is that initial values are need to be selected. Figure 13 illustrates Expectation and Maximization segmentation are used to segment the infected brinjal leaf.

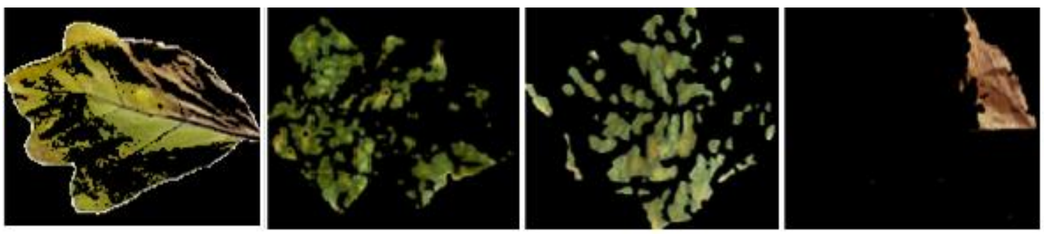

Fig. 13. Expectation Maximization based segmentation

This technique produces strong segmentation results together with the noisy pixels inside the lesion area. However, the primary drawback of this process is the degradation of the affected area based on contour region. An infected brinjal leaf was segmented using an automated spectral lesion approach, as shown in Figure 14.

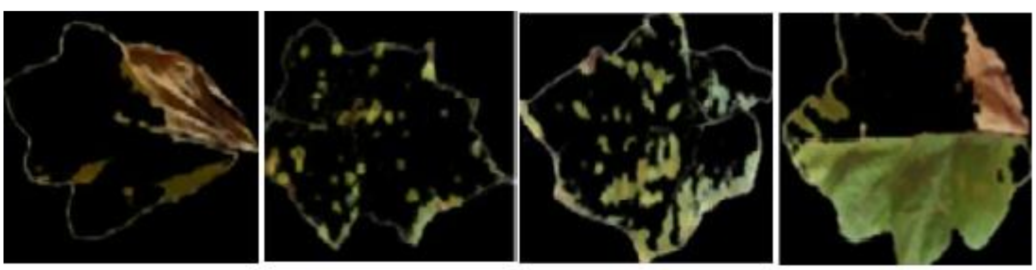

Fig. 14. Automatic Spectral lesion based segmentation

This model beats all the existing methods, even when segmenting in noisy areas. In addition, it provides more flexibility in determining the affected areas of the leaf by producing distinct border detection, which leads to accurate segmentation outcomes and shorter computation times. Table 1 below shows the accuracy of the different segmentation results.

Table 1. Accuracy measures for the segmented results

Segmentation methods	Accuracy			
	Pseudomonas solanacearum	*Cercospora solani*	*Alterneria melongenea*	Tobacco Mosaic virus
FCM	79.13	84.26	86.36	87.43
K-means	89.78	87.45	85.18	87.74

Segmentation methods	Accuracy			
	Pseudomonas solanacearum	*Cercospora solani*	*Alterneria melongenea*	Tobacco Mosaic virus
EM	97.54	94.89	95.67	95.86
ASL	99.79	98.46	98.78	99.89

Automatic Spectral Lesion Based Segmentation generated 99.89 percent of the findings when compared to the other segmentation methods. An image fusion technique is utilized to extract more information by combining Automatic Spectral Lesion Based segmentation and Expectation Maximization segmentation. Image fusion using the discrete wavelet transform is shown in Figure 15.

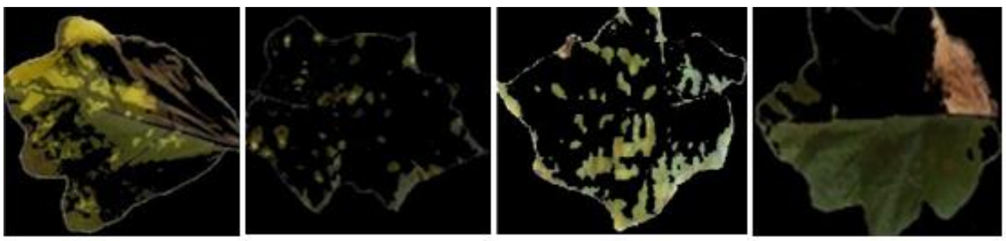

Fig. 15. Discrete Wavelet Transform based image fusion

Even in images with higher contrast, the discrete wavelet transformsbased approach boosted accuracy by utilizing spectral and spatial information. Image fusion using the Dual Tree Complex Wavelet Transform is shown in Figure 16.

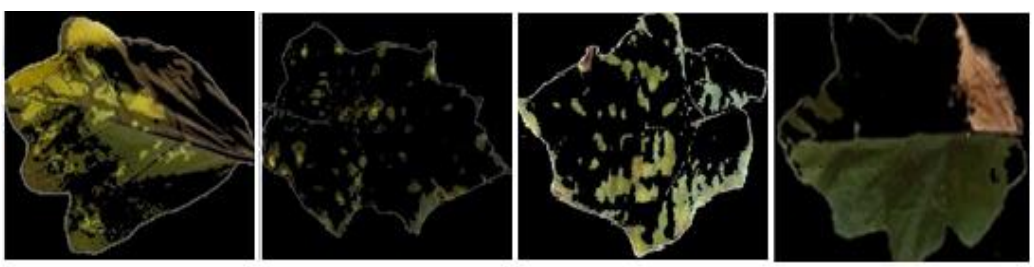

Fig. 16. Dual Tree Complex Wavelet Transform based image fusion

The Dual tree complex wavelet technique generated better outcomes in noisy distortion while maintaining all of the information in the brinjal leaf when compared to the previous fusion findings. Image fusion using the Discrete Shearlet Transform is seen in Figure 17.

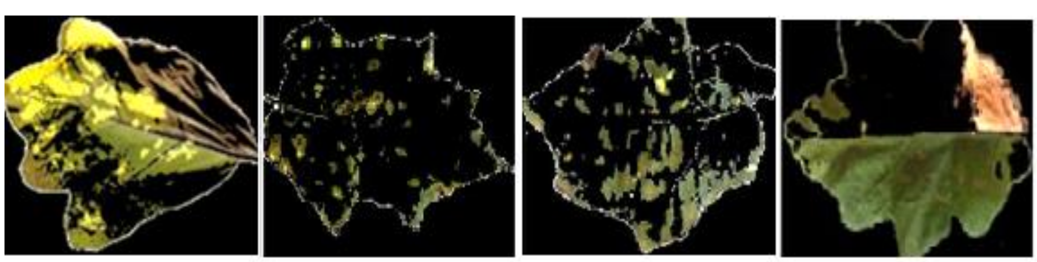

Fig. 17.DiscreteShearlet Transform based image fusion

Discrete Shearlet transformbased image fusion provides detail information, a greater grey level and a sharper image even in the presence of artifacts and fuzzy regions. Table 2 displays the texture characteristic from the fused image.

Tables 2. Texture Feature

Features	*Pseudomonas solanacearum*	*Cercosporasolani*	*Alterneriamelongenea*	Tobacco Mosaic virus
Mean	121.35	143.43	153.75	145.16
SD	118.41	134.14	147.32	135.74
Entropy	4.67	13.13	3.65	4.33
RMS	12.36	3.75	13.66	13.75
Variance	9265	9686	11674	9433
Smoothness	1.01	1	1	1
Kurtosis	2.16	2.57	3.02	2.57
Skewness	0.25	0.032	0.007	-0.053
IDM	255	255	255	255
Contrast	0. 723	0.482	0.468	0.465
Correlation	0.9837	0.9784	0.9799	0.9962
Energy	0.449	0.4567	0.4723	0.4355
Homogeneity	0.9534	0.9724	0.9725	0.9892

As demonstrated in Table 1, contrast features result in a low value for the leaf in *Pseudomonas solanacearum* disease and a value greater than '1' for the other diseases. According to the correlation, photographs of leaves showing *Cercosporasolani* disease have a lower energy value than images of leaves showing *Alterneriamelongenea* disease, which has a higher energy value. For leaf image in *Alterneriamelongenea*, homogeneity results in a low entropy value, however for leaf images with Tobacco Mosaic Virus, it provides a bigger value. Following that, color features like color moment and color histogram descriptors are extracted using the color features. Table 3 illustrates the extraction of colorbased features for fusion approaches.

Table 3. Color features for DST

Diseases	Histogram	Mean	Standard Deviation	Skewness
Pseudomonas solanacearum	0.065	126.34	68.23	-1.34
Cercosporasolani	0.287	136.34	66.34	-1.18
Alterneriamelongenea	0.465	143.23	65.24	-0.92

Diseases	Histogram	Mean	Standard Deviation	Skewness
Tobacco Mosaic virus	0.363	136.23	68.34	-0.64

Table 4. Structural features for DST

Diseases	Asymmetry	Border Irregularity	Color	Diameter
Pseudomonas solanacearum	4.25	0.19	1.76	5.78
Cercosporasolani	2.78	0.32	1.67	3.56
Alterneriamelongenea	2.45	0.16	1.89	7.67
Pythium aphanidermatum	7.23	0.26	2.67	4.35
Tobacco Mosaic virus	3.67	0.65	2.89	3.45

It is evident that DST based fusion is enhancing in terms of both spectral and spatial information under all conditions. The distinction in the severity levels for the brinjal leaf can help to identify the different types of diseases. The feature vector incorporates composite features, including structural, color, and textural aspects to enhance classification accuracy when compared to the individual feature dataset. Figure 18 illustrates the performance of the classifier for the fused image to automatically identify diseases.

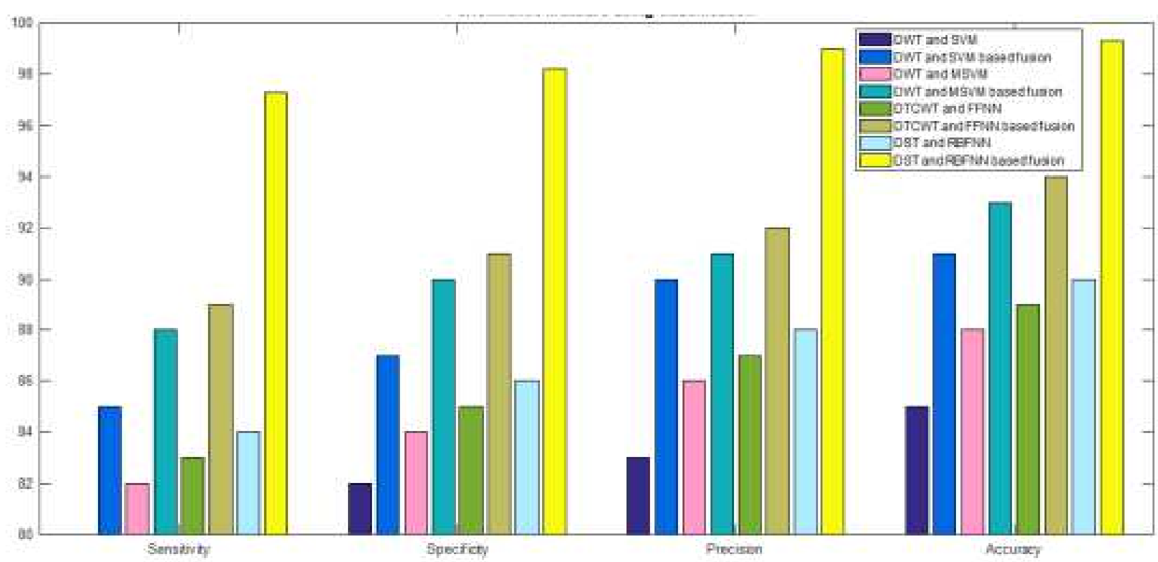

Fig. 18. Performance analysis of classifier with image fusion

The accuracy for the Radial Basis Function Neural Network and the DST based fusion approach is relatively high in comparison to other classification techniques. 99.35% of the samples were classified accurately with 89.24% sensitivity, 94.67% specificity and 90.12% precision. The results are also assessed by the department of agriculture. All the disease results are valid except for Tobacco Mosaic Virus; nonetheless, there is significant variation in the textural feature, especially skewness across the region. All other parameters including mean, standard deviation, kurtosis, IDM, energy, contrast, entropy, RMS, variance, smoothness, correlation, energy, and homogeneity are almost same for the same set of disorders.

5. Conclusion

The research presents DSTbased image fusion along with the feature extraction algorithms that improve on the practicality, efficiency and effectiveness of the Discrete Wavelet Transform and the Discrete Dual Tree Wavelet Transform respectively. Leaf images are characterized by three distinct views through the use of color, texture, and structurebased characteristics. This technique enhanced to provide discriminative image descriptors. In contrast, the disease within the leaf exhibits a uniform hue and texture, despite its diverse structure, which is further highlighted by the location of the lesion area. Specifically, the combination of all unique qualities generates and enhances the classification rate. Additionally, the result demonstrates that the Radial Basis Function Neural Network and the DST execute more accurately. In the future, a handy pocket-sized device and a mobile application may be introduced that analyzes a large region without the need for expert knowledge and provides the illness severity level within the necessary time frame.

References

Reference to a journal publication:

[1]. Tucker, C, and Chakraborty, S. (1997). Quantitative assessment of lesion characteristics and disease severity using digital image processing. Journal of Phytopathology. 145(7), pp. 273-278.

[2]. Al-Hiary, H, Bani-Ahmad, G, Reyalat, M, Braik, M, and Rahamneh, AL. (2011). Fast and accurate detection and classification of plant diseases," International Journal of Computer Applications. 14(6), pp. 31-38.

[3]. Anand, R, Veni, S & Aravinth, J. (2016), An application of image processing techniques for detection of diseases on brinjal leaves using k-means clustering method. International Conference on Recent Trends in Information Technology, ICRTIT. doi.org/10.1109/ ICRTIT. 7569531.

[4]. Skaloudova, B, Krvan, V & Zemek, R.(2006). Computer-assisted estimation of leaf damage caused by spider mites. Computer and Electron Agriculture. 53(2). pp. 81-91.

[5]. Youwen, T, Tianlai, L, and Yan, N. (2008). The recognition of cucumber disease based on image processing and support vector machine. In Congress on Image and Signal Processing. 2. pp. 262–267.

[6]. Camargo, A, and Smith, JS. (2009). Image pattern classification for the identification of disease causing agents in plants. Computers and Electronics in Agriculture. 66(2), pp. 121–125.

[7]. Yao, Q, Guan, Z, Zhou, Y, Tang, J, Hu, Y, and Yang, B. (2009). Application of support vector machine for detecting rice diseases using shape and color texture features. International Conference on Engineering Computation, pp. 79–83.

[8]. Pydipati, R, Burks, TF, and Lee, WS. (2005). Statistical and neural network classifiers for citrus disease detection using machine vision. Transactions of the ASAE. 48(5), pp. 2007–2014.

[9]. Barbedo, JCA. (2013). Digital image processing techniques for detecting, quantifying and classifying plant diseases. Springer Plus, 2(6), pp. 1-12.

[10]. Aji, AF, Munajat, Q, Pratama, AP, Kalamullah, H, Aprinaldi, Setiyawan, J, and Arymurthy, AM .(2013). Detection of palm oil leaf disease with image processing and neural

network classification on mobile device. International Journal of Computer Theory and Engineering. 5(3), pp. 529-532.
[11]. Bhange, M and Hingoliwala, HA. (2015). Smart farming: pomegranate disease detection using image processing. Second International Symposium on Computer Vision and the Internet (VisionNet'15). 58(6), pp. 280-288.
[12]. Singh, V and Misra, AK. (2017). Detection of plant leaf diseases using image segmentation and soft computing techniques. Information Processing in Agriculture. 4(1), pp. 41-49.
[13]. James, WC. (1974). Assessment of plant disease and losses. Annual Review of Phytopathology. 12(1), pp. 27–48.
[13]. Chary, RVR, Lakshmi, DR and Sunitha, KVN. (2012). Feature extraction methods for color image similarity. Advanced Computing: An International Journal. 3(2), pp. 147-157.
[14]. Huang, KY. (2007). Application of artificial neural network for detecting Phalaenopsis seedling diseases using color and texture features. Computers and Electronics in Agriculture. 57(1), pp. 3-11.
[15]. Avci, E and Avci, D. (2008). The performance comparison of discrete wavelet neural network and discrete wavelet adaptive network based fuzzy inference system for digital modulation recognition. Expert Systems with Application. 35(2), pp. 90-101.
[16]. Muthukannan, K, Latha, P, Pon Selvi, R and Nisha, P.N. (2015). Classification of diseased plant leaves using neural network algorithms. ARPN Journal of Engineering and Applied Sciences. 10(4), pp. 1913-1919.
[17]. Zhang, W, Teng, G and Wang, C. (2013). Identification of jujube trees diseases using neural Network. International Journal for Light and Electron Optics. 124(11), pp. 1034-1037.
[18]. Pixia, D and Xiangdong, W. (2013). Recognition of greenhouse cucumber disease based on image processing technology. Open Journal of Applied Sciences. 3(1), pp. 27-31.

Reference to a proceeding:

[19]. Orillo, JW, Cruz, JD, Agapito,, L, and Valenzuela, PJSI. (2013). Identification of diseases in rice plant (Oryza Sativa) using back propagation artificial neural network. 7th IEEE International Conference Humanoid, Nanotechnology, Information Technology Communication and Control, Environment and Management (HNICEM) pp. 1-6.
[20]. Wang, H, Li, G, Ma, Z and Li ,X. (2012). Image Recognition of Plant Disease based on Principal Component Analysis and Neural Network. Eighth International Conference on Natural Computation. 25(9), pp. 246-251.